

Finite-Size Scaling of Non-Gaussian Fluctuations Near the QCD Critical Point

Roy A. Lacey,^{1,2,*} Peifeng Liu,^{1,2} Niseem Magdy,¹ B. Schweid,^{1,2} and N. N. Ajitanand¹

¹*Department of Chemistry, Stony Brook University, Stony Brook, NY, 11794-3400, USA*

²*Dept. of Physics, Stony Brook University, Stony Brook, NY, 11794, USA*

(Dated: November 2, 2016)

An effective Finite-Size Scaling (FSS) of moment products from recent STAR measurements of the variance σ , skewness S and kurtosis κ of net-proton multiplicity distributions, are reported for a broad range of collision centralities in Au+Au ($\sqrt{s_{NN}} = 7.7 - 200$ GeV) collisions. The products $S\sigma$ and $\kappa\sigma^2$, which are directly related to the higher-order baryon number susceptibility ratios $\chi_B^{(3)}/\chi_B^{(2)}$ and $\chi_B^{(4)}/\chi_B^{(2)}$, show scaling patterns consistent with earlier indications for a second order phase transition at a critical end point (CEP) in the plane of temperature vs. baryon chemical potential (T, μ_B) of the QCD phase diagram. The resulting scaling functions validate the earlier estimates of $T^{\text{cep}} \sim 165$ MeV and $\mu_B^{\text{cep}} \sim 95$ MeV for the location of the CEP, and the critical exponents used to assign its 3D Ising model universality class.

PACS numbers: 25.75.Dw

A major experimental theme at both the Super Proton Synchrotron (SPS) [1] and the Relativistic Heavy Ion Collider (RHIC) [2], is the study of observables that could signal the location and character of the critical end point (CEP) – the end point of the first-order coexistence curve in the temperature vs. baryon chemical potential (T, μ_B) plane of the phase diagram for Quantum Chromodynamics (QCD) [3–6]. The first beam energy scan at RHIC ($\sqrt{s_{NN}} = 7.7 - 200$ GeV – BES-I) facilitated measurements spanning a broad domain ($20 < \mu_B < 420$ MeV [7–9]) of this phase diagram.

A common strategy for locating the CEP is to scan the phase diagram by varying the beam collision energy ($\sqrt{s_{NN}}$), and look for non-monotonic behavior of experimental observables sensitive to the proximity of reaction trajectories to the CEP [6, 10–13]. This strategy stems from the fact that, for an infinite volume system, the critical point is characterized by several (power law) divergences linked to the divergence of the correlation length $\xi \propto |t|^{-\nu} \equiv |T - T^{\text{cep}}|^{-\nu}$. Notable examples are the quadratic variances of event-by-event multiplicity distributions for net charge, baryon number, etc, $\langle(\delta n)\rangle \sim \xi^{\gamma/\nu}$, the isobaric heat capacity $C_p \sim \xi^{\gamma/\nu}$ and the isothermal compressibility $\kappa_T \sim \xi^{\gamma/\nu}$; the values of the critical exponents ν and γ [14] can be determined via the static universality class of the CEP.

The higher-order moments of the net-baryon multiplicity distributions, which are related to the higher-order baryon number susceptibilities, are predicted to be even more sensitive to the CEP since they are proportional to higher powers of the correlation length [12, 13]. Thus, the search for an increase/divergence or a non-monotonic trend in the excitation function of net-baryon (net-proton) fluctuations is a favored approach in ongoing experimental efforts to pinpoint the location of the CEP [1, 2, 15–17].

The observation of non-monotonic signatures, while important, is neither necessary nor sufficient for identifi-

cation and full characterization of the CEP. Moreover, finite-size and finite-time effects impose non-negligible constraints on the magnitude of ξ [18]. If the effective correlation length associated with finite-time effects $\hat{\xi} \geq L$, a pseudo-critical point with $\xi > L$, could result from the finite volume ($V \propto L^3$) systems created in heavy ion collisions. Such a pseudocritical point would lead to a characteristic power law volume dependence of the magnitude (χ_T^{max}), width (δT) and peak position ($\bar{\tau}_T$) of the susceptibility and its related observables [19];

$$\chi_T^{\text{max}}(V) \sim L^{\gamma/\nu}, \quad (1)$$

$$\delta T(V) \sim L^{-\frac{1}{\nu}}, \quad (2)$$

$$\bar{\tau}_T(V) \sim T^{\text{cep}}(V) - T^{\text{cep}}(\infty) \sim L^{-\frac{1}{\nu}}, \quad (3)$$

where ν and γ are critical exponents which characterize the divergence of ξ and χ_T respectively. Therefore, the reduction of the magnitude of $\chi_T^{\text{max}}(V)$ ($\chi_{\mu_B}^{\text{max}}(V)$), broadening of the transition region $\delta T(V)$ ($\delta \mu_B(V)$) and the shift of $T^{\text{cep}}(\mu_B^{\text{cep}})$, which all increase as the volume decreases, provide a unique set of finite-size signatures for locating and characterizing the CEP [19–23].

In general, the i th order susceptibility can be written in a finite-time-finite-size scaling form as [24–26];

$$\chi^{(i)}(\tau, t, L) \sim L^3 b^{i\delta\beta/\nu} \chi^{(i)}(\tau b^{1/\nu}, t b^{-z}, L^{-1}b), \quad (4)$$

where b is the renormalization-group scale factor, z is the dynamic critical exponent and δ and β are additional static critical exponents. A suitable choice of the scale factor b gives

$$\chi^{(i)} \sim L^{3+i\delta\beta/\nu} f_1(\tau L^{1/\nu}, R L^r), \quad (5)$$

and

$$\chi^{(i)} = L^3 R^{-i\delta\beta/r\nu} f_2(\tau R^{-1/r\nu}, L^{-1} R^{-1/r}), \quad (6)$$

for the Finite-Size Scaling (FSS) and Finite-Time Scaling (FTS) forms respectively. Here, $r = z + 1/\nu$ and R can

be associated with a cooling rate which drives the system from an initial temperature T_i through the critical temperature T_{cep} [26].

The regime of FSS is satisfied for $L^{-1}R^{-1/r} \gg 1$ and $\tau R^{-1/\nu} = \tau L^{1/\nu} (L^{-1}R^{-1/r})^{1/\nu} \ll 1$, and the ratio of susceptibilities can be expressed as;

$$\frac{\chi^{(n)}}{\chi^{(m)}} = L^{(n-m)\delta\beta/\nu} f(\tau L^{1/\nu}). \quad (7)$$

The regime of FTS is restricted to $L^{-1}R^{-1/r} \ll 1$ or $R^{-1/r} \ll L$. Therefore, if finite-time effects dominate, $\xi > L > \hat{\xi}$ and $\chi^{(n)}/\chi^{(m)}$ will be essentially independent of L (*i.e.* $(n-m)\delta\beta/\nu \sim 0$) and $\chi^{(i)} \sim L^3$. Eq.7 implies that an observable related to the susceptibility ratio $\chi^{(n)}/\chi^{(m)}$, obtained for different system sizes, can be re-scaled to the non-singular scaling function $f(\tau L^{1/\nu})$. That is, FSS for different values of L , should lead to data collapse onto a single curve for robust values of T^{cep} , μ_B^{cep} and the associated critical exponents;

$$\begin{aligned} \frac{\chi^{(n)}}{\chi^{(m)}} L^{(m-n)\delta\beta/\nu} \text{ vs. } t_T L^{1/\nu}, \\ \frac{\chi^{(n)}}{\chi^{(m)}} L^{(m-n)\delta\beta/\nu} \text{ vs. } t_{\mu_B} L^{1/\nu}, \end{aligned} \quad (8)$$

where $\tau_T = (T - T^{\text{cep}})/T^{\text{cep}}$ and $\tau_{\mu_B} = (\mu_B - \mu_B^{\text{cep}})/\mu_B^{\text{cep}}$ are the reduced temperature and baryon chemical potential respectively. A further simplification of these expressions results from the influence of finite-time effects which render the exponent for L on the left-hand side of Eq. 8, $(m-n)\delta\beta/\nu \sim 0$.

In recent work [22, 23], the centrality dependent excitation functions for the Gaussian emission source radii difference ($R_{\text{out}}^2 - R_{\text{side}}^2 = \Delta R^2$), obtained from two-pion interferometry measurements in Au+Au ($\sqrt{s_{NN}} = 7.7 - 200$ GeV) and Pb+Pb ($\sqrt{s_{NN}} = 2.76$ TeV) collisions, were employed to search for the CEP; ΔR^2 can be linked to a susceptibility, given its connection to the compressibility [22, 23]. The observed non-monotonic excitation functions validated the characteristic finite-size scaling patterns expected for a deconfinement phase transition and the CEP. The ensuing Finite-Size Scaling analysis of these data [22, 23] indicated a second order phase transition with $T^{\text{cep}} \sim 165$ MeV and $\mu_B^{\text{cep}} \sim 95$ MeV for the location of the critical end point, as well as critical exponents ($\nu = 0.66 \pm 0.05$ and $\gamma = 1.15 \pm 0.065$) which placed the CEP in the 3D Ising model universality class. However, it remains an open question as to whether these findings are consistent with the fluctuation measurements (especially net-proton fluctuations) obtained in the same experiments.

In this work, we investigate whether the estimates for T^{cep} , μ_B^{cep} and the associated critical exponents reported in Refs. [22, 23], lead to robust Finite-Size Scaling of recent STAR measurements of the beam energy and centrality dependent moment products $S\sigma$ and $\kappa\sigma^2$, for net-protons. Here, σ , S and κ are the variance, skewness and

kurtosis (respectively) of the event-by-event net-proton multiplicity distributions. We find clear evidence for an effective Finite-Size Scaling of $S\sigma$ and $\kappa\sigma^2$, compatible with the location and properties of the CEP reported in Refs. [22, 23].

The efficiency corrected data employed in the present analysis, are obtained from centrality dependent fluctuation measurements ($0.4 < p_T < 0.8$ GeV/c and $|y| < 0.5$) reported by the STAR collaboration for Au+Au collisions spanning the range $\sqrt{s_{NN}} = 7.7 - 200$ GeV [15]. The moment products ($S\sigma$ and $\kappa\sigma^2$) which are obtained from the cumulants of the net-proton multiplicity distributions, $C_3/C_2 = S\sigma$ and $C_4/C_2 = \kappa\sigma^2$, are related to the ratio of baryon number susceptibilities, $S\sigma \sim \chi_B^{(3)}/\chi_B^{(2)}$ and $\kappa\sigma^2 \sim \chi_B^{(4)}/\chi_B^{(2)}$ [27–30]. The systematic uncertainties for these measurements are reported to be of order 4% for σ , 5% for S and 12% for κ [15]. The reported statistical uncertainties are in general, much larger for $\kappa\sigma^2$ than for $S\sigma$. Note as well that it is assumed that the shape of the net-proton distributions reflects the net-baryon distributions up to distortions smaller than the estimated uncertainties for the cumulant measurements.

The size parameter $\bar{R} = L$, employed in our Finite-Size Scaling analysis is obtained from a Monte Carlo Glauber (MC-Glauber) calculation [31–33], performed for several collision centralities at each beam energy. In each of these calculations, a subset of the nucleons become participants (N_{part}) in each collision by undergoing an initial inelastic N+N interaction. The transverse distribution of these participants in the X-Y plane has RMS widths σ_x and σ_y along its principal axes. We define and compute \bar{R} , the characteristic initial transverse size, as $1/\bar{R} = \sqrt{(1/\sigma_x^2 + 1/\sigma_y^2)}$ [34]. Here, it is noteworthy that the three HBT radii R_{out} , R_{side} and R_{long} , which serve to characterize the space-time dimensions of the emitting sources in Au+Au collisions over the same span of beam energies, all show a linear dependence on \bar{R} [35, 36]. The systematic uncertainties for \bar{R} , obtained via variation of the model parameters, are less than 10% [32, 33].

Validation tests for finite-size scaling of the moment products $S\sigma \sim \chi_B^{(3)}/\chi_B^{(2)}$ and $\kappa\sigma^2 \sim \chi_B^{(4)}/\chi_B^{(2)}$ were carried out for the full set of centrality dependent measurements as follows. First, we exploit the phenomenology of thermal models [7–9] for the freeze-out region and use the $\sqrt{s_{NN}}$ values to obtain the corresponding T and μ_B values [7]. We then use the previously extracted [22] values of $T^{\text{cep}} \sim 165$ MeV and $\mu_B^{\text{cep}} \sim 95$ MeV to obtain t_T and t_{μ_B} over the full range of the measurements. Subsequently, the value $\nu \sim 0.66$ [22] and those for \bar{R} (L) were used in conjunction with Eq. 8 and $(m-n)\delta\beta/\nu \sim 0$, to test for collapse of the centrality dependent data onto a single curve. Here, $(m-n)\delta\beta/\nu \sim 0$ takes account of the strong influence of finite-time effects, given the large value of $z = 3$, for the thermal slow mode which drives the critical dynamics associated with fluctuations

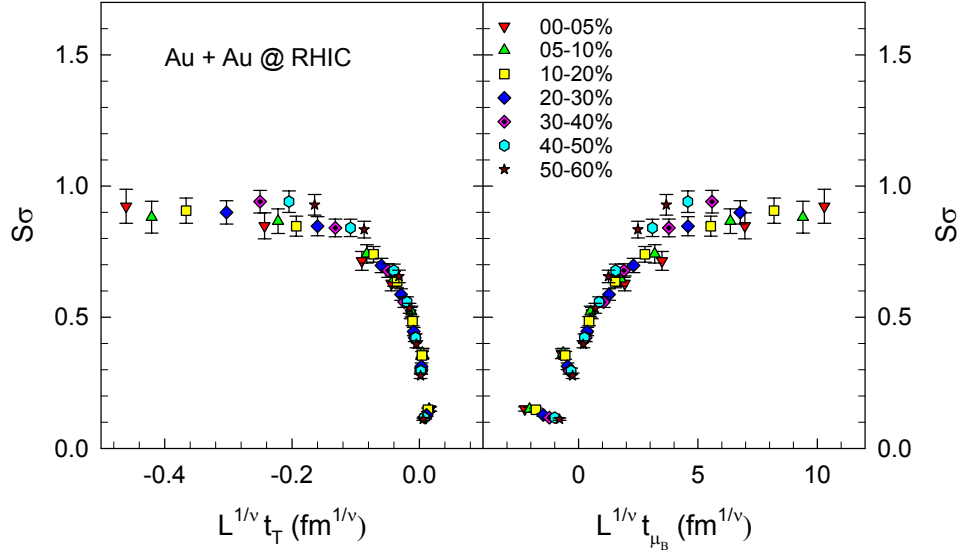


FIG. 1. $S\sigma$ vs. $L^{1/\nu}t_T$ (left panel) and $L^{1/\nu}t_{\mu_B}$ (right panel) for 0-5%, 5-10%, 10-20%, 20-30%, 30-40%, 40-50% and 50-60% Au+Au collisions for $0.4 < p_T < 0.8$ GeV and $|y| < 0.5$. The efficiency corrected data are taken from Ref. [15]; scaling was performed with $T^{\text{cep}} \sim 165$ MeV, $\mu_B^{\text{cep}} \sim 95$ MeV and $\nu \sim 0.66$ [22, 23].

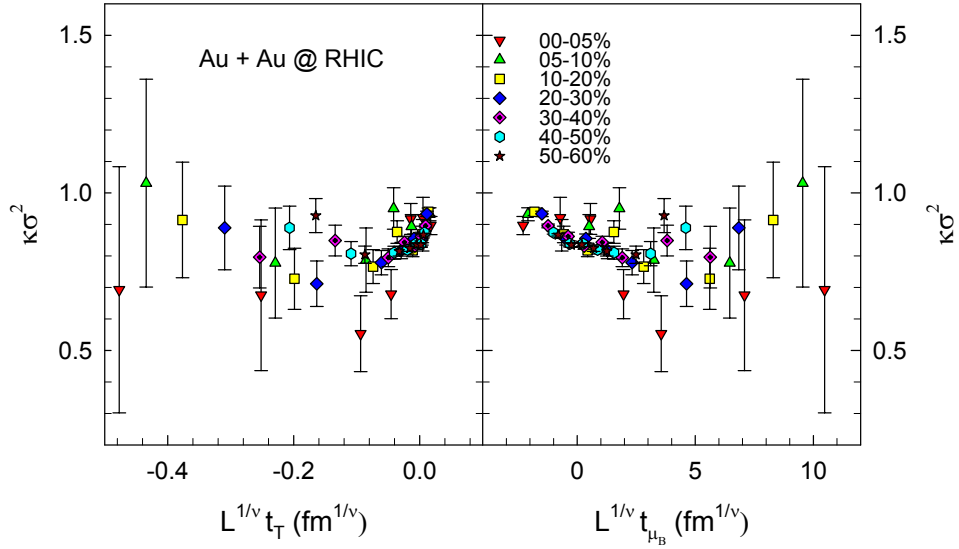


FIG. 2. $\kappa\sigma^2$ vs. $L^{1/\nu}t_T$ (left panel) and $L^{1/\nu}t_{\mu_B}$ (right panel) for 0-5%, 5-10%, 10-20%, 20-30%, 30-40%, 40-50% and 50-60% Au+Au collisions for $0.4 < p_T < 0.8$ GeV and $|y| < 0.5$. The efficiency corrected data are taken from Ref. [15]; scaling was performed with $T^{\text{cep}} \sim 165$ MeV, $\mu_B^{\text{cep}} \sim 95$ MeV and $\nu \sim 0.66$ [22, 23].

[18, 37]. This influence was further validated via the scaling functions expected for $L^{-3}\chi^{(i)}$ vs. $f(\tau L^{1/\nu})$.

Figures 1 and 2 show the results of the FSS tests for $S\sigma$ and $\kappa\sigma^2$ respectively. The left and right panel in each figure, show results for the scaled variable $t_T L^{1/\nu}$ and $t_{\mu_B} L^{1/\nu}$ respectively. Both figures indicate data collapse onto a single curve for the indicated values of T^{cep} , μ_B^{cep} and ν , albeit with much less statistical significance for $\kappa\sigma^2$ (cf. Fig. 2), especially for T (μ_B) values smaller (larger) than T^{cep} (μ_B^{cep}). The resulting scaling functions

for $S\sigma$ and $\kappa\sigma^2$ also indicate characteristic shape differences akin to those for the 3D Ising model.

The scaling functions in Figs. 1 and 2 point to the efficacy of Finite-Size Scaling as a tool to locate and characterize the CEP. They indicate that the non-Gaussian fluctuations for net-protons, quantified by $S\sigma$ and $\kappa\sigma^2$ respectively, are consistent with the critical fluctuations expected for reaction trajectories close to a second order phase transition at a CEP located at $T^{\text{cep}} \sim 165$ MeV and $\mu_B^{\text{cep}} \sim 95$ MeV, belonging to the 3-D Ising Model

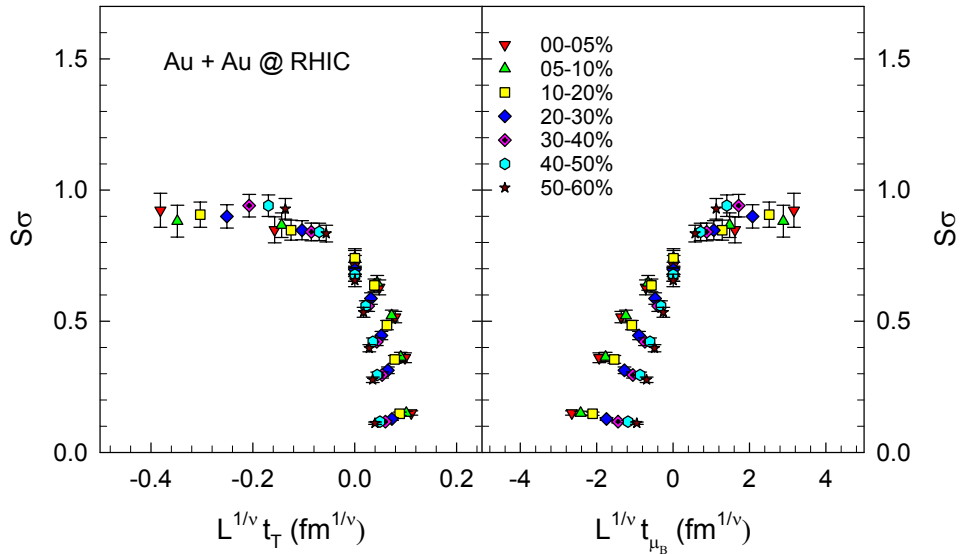


FIG. 3. Same as Fig. 1, for the test values $\hat{T}^{\text{cep}} \sim 160$ MeV and $\mu_B^{\text{cep}} \sim 205$ MeV ($\sqrt{s_{NN}} \sim 20$ GeV).

universality class [22, 23].

It is often argued that theoretical and experimental estimates limits the location of the CEP to μ_B^{cep} values larger than 200 MeV [17, 38]. Consequently, it is instructive to perform scaling tests with μ_B^{cep} and T^{cep} values different from the ones used for the scaling tests shown in Figs. 1 and 2, *i.e.*, different from the values reported in Ref. [22]. The results from one such test are shown in Fig. 3 for the *test* values $\hat{T}^{\text{cep}} \sim 160$ MeV and $\mu_B^{\text{cep}} \sim 205$ MeV. These values correspond to chemical freeze-out at $\sqrt{s_{NN}} \sim 20$ GeV, where minima/maxima in the non-monotonic patterns for several observables have been reported [17, 35, 36, 39, 40].

In contrast to Figs. 1 and 2, Fig. 3 clearly shows that Finite-Size Scaling is broken, indicating that the *test* values \hat{T}^{cep} and μ_B^{cep} do not constitute a good estimate for the location of the CEP. Similar results were obtained for other \hat{T}^{cep} and μ_B^{cep} values, corresponding to even smaller values of $\sqrt{s_{NN}}$, *i.e.*, smaller values of T^{cep} and larger value of μ_B^{cep} .

In summary, we have performed validation tests for effective Finite-Size Scaling of recent STAR measurements of the excitation function for non-Gaussian fluctuations, characterized by the moment products $S\sigma$ and $\kappa\sigma^2$ of the event-by-event net-proton multiplicity distributions. The scaling tests, which provide a potent tool for locating and characterizing the CEP, validate characteristic FSS patterns consistent with a second order deconfinement phase transition at the critical end point. They also indicate consistency with the earlier estimate [22, 23] of $T^{\text{cep}} \sim 165$ MeV and $\mu_B^{\text{cep}} \sim 95$ MeV for the location of the CEP, and the critical exponents used to assign its 3D Ising Model universality class. Further detailed studies at RHIC, with the slated STAR detector upgrades and RHIC beam intensity enhancements – especially for the

low energy beams, are crucial to firm-up the precise location of the CEP, and the values of the critical exponents required for its precise characterization.

ACKNOWLEDGMENTS

The authors thank Jiangyong Jia, and Zhangbu Xu for valuable discussions. This research is supported by the US DOE under contract DE-FG02-87ER40331.A008.

* E-mail: Roy.Lacey@Stonybrook.edu

- [1] T. Anticic et al. (NA49), Phys. Rev. **C81**, 064907 (2010), 0912.4198.
- [2] H. Caines (STAR), in *QCD and high energy interactions. Proceedings, 44th Rencontres de Moriond, La Thuile, Italy, March 14-21, 2009* (2009), pp. 375–378, 0906.0305.
- [3] N. Itoh, Prog. Theor. Phys. **44**, 291 (1970).
- [4] E. V. Shuryak, CERN-83-01 (1983).
- [5] M. Asakawa and K. Yazaki, Nucl. Phys. **A504**, 668 (1989).
- [6] M. A. Stephanov, K. Rajagopal, and E. V. Shuryak, Phys. Rev. Lett. **81**, 4816 (1998), hep-ph/9806219.
- [7] J. Cleymans, H. Oeschler, K. Redlich, and S. Wheaton, J.Phys. **G32**, S165 (2006), hep-ph/0607164.
- [8] A. Andronic, P. Braun-Munzinger, and J. Stachel, Acta Phys.Polon. **B40**, 1005 (2009), 0901.2909.
- [9] F. Becattini, M. Bleicher, T. Kollegger, M. Mitrovski, T. Schuster, et al., Phys.Rev. **C85**, 044921 (2012), 1201.6349.
- [10] M. A. Stephanov, Prog. Theor. Phys. Suppl. **153**, 139 (2004), [Int. J. Mod. Phys.A20,4387(2005)], hep-ph/0402115.
- [11] M. Asakawa, S. Ejiri, and M. Kitazawa, Phys. Rev. Lett. **103**, 262301 (2009), 0904.2089.

- [12] M. A. Stephanov, Phys. Rev. Lett. **102**, 032301 (2009), 0809.3450.
- [13] C. Athanasiou, K. Rajagopal, and M. Stephanov, Phys. Rev. **D82**, 074008 (2010), 1006.4636.
- [14] The critical exponents satisfy several equalities. Thus, only two of the four exponents are independent.
- [15] L. Adamczyk et al. (STAR), Phys. Rev. Lett. **112**, 032302 (2014), 1309.5681.
- [16] X. Luo, B. Mohanty, and N. Xu, Nucl. Phys. **A931**, 808 (2014), 1408.0495.
- [17] X. Luo, in *25th International Conference on Ultra-Relativistic Nucleus-Nucleus Collisions (Quark Matter 2015) Kobe, Japan, September 27-October 3, 2015* (2015), 1512.09215, URL <https://inspirehep.net/record/1411819/files/arXiv:1512.09215.pdf>.
- [18] B. Berdnikov and K. Rajagopal, Phys. Rev. **D61**, 105017 (2000), hep-ph/9912274.
- [19] M. Ladrem and A. Ait-El-Djoudi, Eur.Phys.J. **C44**, 257 (2005), hep-ph/0412407.
- [20] L. Palhares, E. Fraga, and T. Kodama, J.Phys. **G38**, 085101 (2011), 0904.4830.
- [21] L.-Z. Chen, Y.-Y. Chen, and Y.-F. Wu, Chin. Phys. **C38**, 104103 (2014), 1002.4139.
- [22] R. A. Lacey, Phys. Rev. Lett. **114**, 142301 (2015), 1411.7931.
- [23] R. A. Lacey (2015), 1512.09152.
- [24] M. Suzuki, Prog. Theor. Phys. **58**, 1142 (1977).
- [25] X. S. Chen, V. Dohm, and A. L. Talapov, Physica A, **232**, 375 (1996).
- [26] Y. Huang, S. Yin, B. Feng, and Z. F., Phys.Rev.B **89**, 054307 (2014).
- [27] S. Ejiri, F. Karsch, and K. Redlich, Phys. Lett. **B633**, 275 (2006), hep-ph/0509051.
- [28] M. Cheng et al., Phys. Rev. **D79**, 074505 (2009), 0811.1006.
- [29] S. Gupta, X. Luo, B. Mohanty, H. G. Ritter, and N. Xu, Science **332**, 1525 (2011), 1105.3934.
- [30] R. V. Gavai and S. Gupta, Phys. Lett. **B696**, 459 (2011), 1001.3796.
- [31] M. L. Miller, K. Reygers, S. J. Sanders, and P. Steinberg, Ann. Rev. Nucl. Part. Sci. **57**, 205 (2007).
- [32] R. A. Lacey, R. Wei, N. Ajitanand, and A. Taranenko, Phys.Rev. **C83**, 044902 (2011), 1009.5230.
- [33] A. Adare et al. (PHENIX Collaboration) (2013), 1310.4793.
- [34] R. Bhalerao, J.-P. Blaizot, N. Borghini, and J.-Y. Ollitrault, Phys.Lett. **B627**, 49 (2005), nucl-th/0508009.
- [35] R. A. Lacey (2014), 1408.1343.
- [36] A. Adare et al. (PHENIX Collaboration) (2014), 1410.2559.
- [37] Y. Minami, Phys. Rev. **D83**, 094019 (2011), 1102.5485.
- [38] F. Karsch et al., in *25th International Conference on Ultra-Relativistic Nucleus-Nucleus Collisions (Quark Matter 2015) Kobe, Japan, September 27-October 3, 2015* (2015), 1512.06987.
- [39] L. Adamczyk et al. (STAR), Phys. Rev. Lett. **112**, 162301 (2014), 1401.3043.
- [40] L. Adamczyk et al. (STAR), Phys. Rev. Lett. **116**, 112302 (2016), 1601.01999.